Journal of Materials Chemistry A

Accepted Manuscript

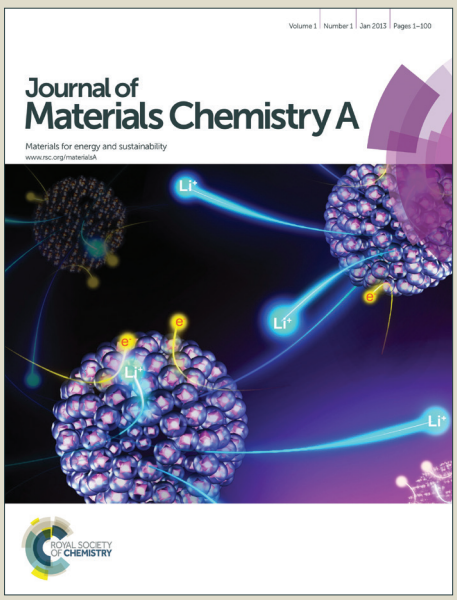

ROYAL SOCIETY OF CHEMISTRY

www.rsc.org/materialsA

Cite this: DOI: 10.1039/c0xx00000x

www.rsc.org/xxxxxx

ARTICLE TYPE

Controllable Synthesis of Cube-like $ZnSnO_3$@TiO_2 Nanostructures as Lithium Ion Batteries Anodes

Yu-ling Qin[a,c], Fei-fei Zhang[a,c], Xin-chuan Du[a,c], Gang Huang[a,c], Ya-cheng Liu[a,c], Li-min Wang[*,a,b]

Received (in XXX, XXX) Xth XXXXXXXXX 20XX, Accepted Xth XXXXXXXXX 20XX

DOI: 10.1039/b000000x

$ZnSnO_3$ is an attractive anode material for lithium ion batteries, because it has a higher theoretical capacity than the state-of-the-art carbonaceous counterpart. The main challenges associated with $ZnSnO_3$ anodes are structural degradation and instability of the solid-electrolyte interphase caused by the large volume change during cycling. Herein, we propose a hierarchical structured $ZnSnO_3$@TiO_2 nanocomposite anode that tackles this problem. The as-prepared core-shell cube-like anode material exhibits the enhanced capacity and cycling property. As a proof-of-concept, this hierarchical heterostructure shows a high initial discharge capacity of 1590 mAh g^{-1} at 100 mA g^{-1}, and retained at 780 mAh g^{-1} after 200 cycles, which is much better than the anodes made of pure $ZnSnO_3$ nanomaterials. The enhanced cycle life can be attributed to the reductive volume expansion during the repeated charge-discharge cycles owing to the hierarchical porous three-dimension structure and TiO_2 shell as well as the synergistic effects of $ZnSnO_3$ and TiO_2.

Introduction

The exploration of suitable electrode materials has been treated as a critical technology to meet the increasing requirements of powerful lithium-ion batteries (LIBs).[1] Efforts to design and search new electrode materials with high energy density and safe cycle life have never ceased. $ZnSnO_3$, as a multifunctional ternary metal oxide material, has long been seemed as a famous functional material in both chemical and physical fields, such as lead-free ferroelectics, transparent conductors, photo-catalysts, dye-sensitized solar cells and gas sensors.[2] In very recent years, it has been considered as a great potential anode candidate for the application in LIBs, due to its higher theoretical capacity (1317 mA h g^{-1}) than the carbonaceous counterpart, low working potential, and its abundance in earth.[3] More importantly, as a bimetal oxide, it also has higher intrinsically superiority than the single metal ZnO and SnO_2, especially its adjustable working potential and increased electronic conductivity.[4]

There are some reports that $ZnSnO_3$ nanoparticles were investigated successfully as an anode material for the application in LIBs. Wang and his partners prepared $ZnSnO_3$ nanocube and nanosheet for LIBs separately, which exhibit the same capacity at the initial cycle. However, the sheet-like $ZnSnO_3$ show the higher capacity (625 mA h g^{-1}) than cube-like $ZnSnO_3$ after 50 cycles.[5a] Using amorphous $ZnSnO_3$ hollow nanoboxes, Dun etc find that they holds a high initial reversible capacity of 661 mA h g^{-1} at 0.1 A g^{-1} rate and acceptable rate performance.[5b] With the help of Co-doped and graphene-carbon, Zn_2SnO_4-based nanocomposite exhibits a reversible capacity of 699 mAh g^{-1} after 50 cycles at 100 mA g^{-1}.[5c]

Although $ZnSnO_3$ with various structures show attractive properties in LIBs, the limited exploration in this area still far from practical application. Particle fracture and loss of electrical contact deriving from serious pulverization and agglomeration of active particles during discharge-charge cycling have been identified as principal reasons for the capacity fading of $ZnSnO_3$ anodes.[3a] Despite the porous structure could decrease this large volume expansion to some extent, the capacity of LIBs still fade away seriously in the long cycle (> 50 cycle).

On the other hand, TiO_2 is also considered as one of the most useful anode materials, due to its excellent structural stability, long-term cycle life, higher safety and environmentally benign.[6] However, the relatively low electronic conductivities and low practical capacity (167 mAh g^{-1} of theoretical capacity) still severely hinder the further application of TiO_2 as a LIBs anode material.[7] In view of this, TiO_2 is usually used to be an auxiliary material to improve the structural stability and cycle life of other anode materials, with partial sacrifice of whole anode capacity.[8] However, using TiO_2 to improve the LIBs performance of $ZnSnO_3$ has been reported.

Herein, a simple co-deposition method is employed to synthesize cube-like $ZnSnO_3$ porous structure. To improve the structural stability and cycle life, TiO_2 is used to coat the $ZnSnO_3$ nanoparticles, forming the $ZnSnO_3$@TiO_2 nanocomposite with $ZnSnO_3$-core and TiO_2-shell. Interestingly, the as-prepared nanocomposite still keeps the cube-like structure after the TiO_2 encapsulation. As a result, the hierarchical heterostructure exhibits a higher initial discharge capacity of 1590 mAh g^{-1} at 100 mA g^{-1}. The discharge capacity still retains 780 mAh g^{-1} after 200 cycles, which is more outstanding than the naked $ZnSnO_3$ anode material. The Coulombic efficiency of $ZnSnO_3$@TiO_2 composite is also higher than that of $ZnSnO_3$.

Experimental

Synthesis of cube-like $ZnSnO_3$ nanoparticles

All reagents were purchased from Aladdin Reagent (China) Co., Ltd. In a typical method to prepare cube-like $ZnSnO_3$ nanoparticles, 5 mmol of zinc sulfate heptahydrate ($ZnSO_4 \cdot 7H_2O$) were added into 100 mL of deionized water with drastically stirring at room temperature. 10 min later, 15 mL of potassium stannate (K_2SnO_3, 5 mmol) solution was poured into zinc sulfate heptahydrate solution. The mixed solution was vigorously stirred at room temperature for 6 h. Then the precipitates were collected by centrifugation and washed with deionized water and ethanol for 6 times. The final $ZnSn(OH)_6$ products were then dried in air at 60 °C. After that, the dry products underwent thermolysis under air with a heating rate of 5 °C min^{-1} from room temperature to 450 °C. Subsequently, the material was calcined for 3 h and then naturally cooled down to room temperature. Finally, white $ZnSnO_3$ nanostructures can be obtained.

Synthesis of $ZnSnO_3$@TiO_2 nanoparticles

1 mmol of $ZnSn(OH)_6$ was dispersed in 50 mL of water, and then 0.4 mL of Dihydroxybis(ammonium lactate)titanium(iv) (DALT, 50 wt% solution in water, Alfa) and 1 mL of aqueous NaOH (0.2 mmol) were added. The dispersion was stirred at room temperature for 2 h. The white particles were obtained by centrifugation and washed with deionized water and ethanol 6 times. After drying at 60 °C overnight, the white products underwent thermolysis under air with a heating rate of 5 °C min^{-1} from room temperature to 450 °C and kept for 3 h. Finally, $ZnSnO_3$@TiO_2 nanostructures can be obtained after the products were cooled down to room temperature naturally.

Characterization

Scanning electron microscopy (SEM) images were produced using a Hitachi S-4800 field emission scanning electron microscope at an accelerating voltage of 10 kV. Transmission electron microscopy (TEM), high-angle annular dark-field scanning transmission electron microscopy (HAADF-STEM) and element mapping were performed on a FEI Tecnai G2 S-Twin instrument with a field emission gun operating at 200 kV. N_2 adsorption-desorption measurements were conducted on a Micromeritics ASAP 2010 instrument at 196 °C after the sample was pretreated at 160 °C for 2 h under vacuum. X-ray photoelectron spectrometry (XPS) spectra were obtained with an ESCALABMKLL X-ray photoelectron spectrometer using an Al Kα source. Powder X-ray diffraction (XRD) patterns were collected on Bruker D8 Focus Powder X-ray diffractometer using Cu Kαradiation (40 kV, 40 mA).

Electrochemical measurements

The electrochemical behaviour of the $ZnSnO_3$@TiO_2 nanoparticles was examined by using CR 2025 coin-type cells with pure lithium foil as the counter electrode, Celgard 2400 membrane as the separator, 1 M $LiPF_6$ dissolved in ethyl carbonate and diethyl carbonate (1:1, wt/wt) as the electrolyte. The working electrode was prepared by compressing a mixture of the active materials, carbon black and sodium alginate with a weight ratio of 70: 20: 10 on to a copper foil and dried in a vacuum oven at 70 °C for 12 h. In this situation, the mass loading ($ZnSnO_3$@TiO_2) per anode plate in the battery is ~0.9 mg cm^{-2}. Then the cells were assembled in a glove box filled with highly pure argon gas. The charge-discharge performance was tested between 0.01 - 3 V, using the LAND CT2001A multi-channel battery testing system at room temperature. The cyclic voltammogram (CV) measurements were conducted on a BioLogic VMP3 Electrochemical Workstation at a scan rate of 0.1 mV s^{-1} in a potential range of 0 - 3 V *vs.* Li/Li^+. Electrochemical impedance spectroscopy (EIS) measurements also performed on BioLogic VMP3 Electrochemical Workstation.

Results and discussion

Structural characterization

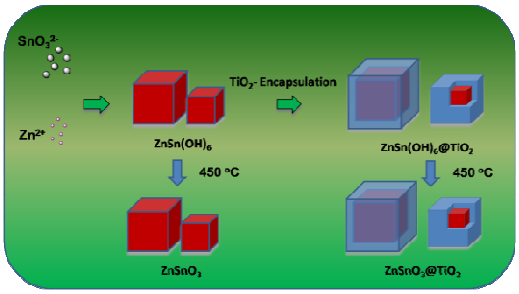

Scheme 1 Schematic of the procedure for preparation of cube-like $ZnSnO_3$ and $ZnSnO_3$@TiO_2.

As is shown in Scheme 1, the typical $ZnSnO_3$@TiO_2 core-shell composite structure is mainly obtained in two steps. Firstly, cube-like $ZnSn(OH)_6$ nanoparticles are formed facilely through mechanical mixing the aqueous K_2SnO_3 and $ZnSO_4$ solution. After that, $ZnSnO_3$ nanoparticles are obtained from the thermal treatment of the prepared $ZnSn(OH)_6$ precursor at 450 °C. Based on the previous results, a cube-like morphological evolution mechanism of the products will not be described here.[5a,2f] Subsequently, a layer of amorphous TiO_2 fully enwraps the $ZnSn(OH)_6$ via Ti-precursor (DALT) chemical bath deposition, forming $ZnSn(OH)_6$@TiO_2 core-shell structure. Finally, a calcinating process at 450 °C in air is employed to convert the as-prepared precursor into $ZnSnO_3$@TiO_2 core-shell composites. The atomic ratio of Zn : Sn : Ti measured by energy dispersive spectroscopy is 38.98 : 39.57 : 21.45.

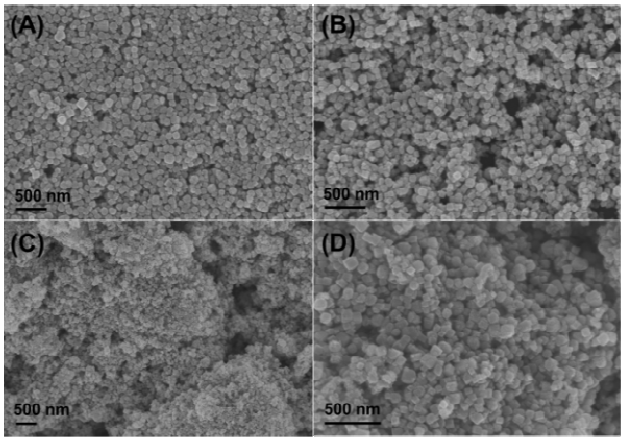

Fig. 1 SEM images of the (A) $ZnSn(OH)_6$, (B) $ZnSnO_3$, C) and (D) $ZnSnO_3$@TiO_2.

Typical SEM images are employed to provide insight into the morphologies of the as-prepared ZnSn-based products obtained in different condition. As is shown in Fig. 1A, the uniform cube-like nanoparticles are successfully obtained by this method. From Fig. 1B, there is no obvious change on the morphology of the nanoparticles after the thermal treatment (450 ^{o}C). Furthermore, the as-prepared ZnSn-based nanoparticles are heated at 150 ^{o}C, 300 ^{o}C and 600 ^{o}C separately, as is shown in Figure S1, which all display the cube-like structure, indicating that the morphology of the nanoparticles would not be destroyed by thermal treatment (< 600 ^{o}C). Fig. 1C and D show that the composite nanoparticles still keep the cube-like structure after the TiO_2-encapsulation.

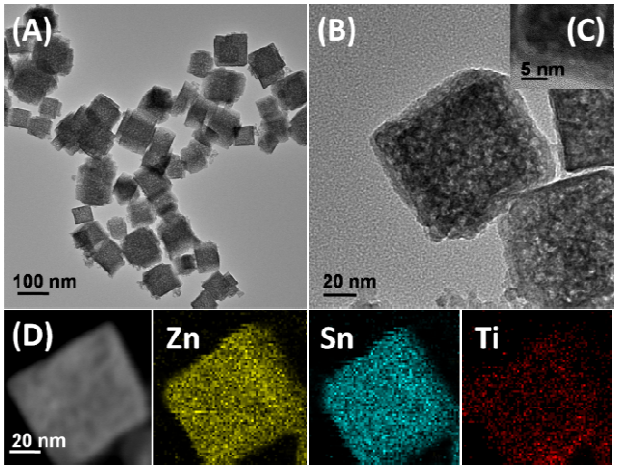

Fig. 2 TEM images of the $ZnSnO_3$@TiO_2 (A, B), HR-TEM image of the $ZnSnO_3$@TiO_2 (C), HAADF-STEM image and element mapping of $ZnSnO_3$@TiO_2 (D).

On the other hand, TEM and HRTEM images are prepared to characterize the detailed structure of the $ZnSnO_3$@TiO_2 composites. As shown in Fig. 2A and B, the as-prepared $ZnSnO_3$@TiO_2 is totally cube-like nanoparticles with porous structure. N_2 adsorption-desorption isotherms and pore size distribution in Figure S2 confirm the porous structure again. The BET surface area is 89 m^2 g^{-1}. The pore size distribution calculated from the desorption data shows that the pore size of the $ZnSnO_3$@TiO_2 mainly centers at ~4 nm. Furthermore, from Fig. 2B, in contrast with its darker central part, the colour of edges on the nanoparticles is lighter, implying the possibility of the formation of core-shell structure. HRTEM image in Fig. 2C shows the marginal part of the nanoparticles, which the obvious boundary line between edge and inside could be found, revealing the core-shell structure again. Element mapping of $ZnSnO_3$@TiO_2 (Fig. 2D) displays the core-shell structure in more detail. Clearly, Zn and Sn atoms are mainly located in the centre of the nanoparticle, while the Ti atoms are distributed in the whole particle. Therefore, the particle with ZnSn-based core and Ti-based shell can be concluded.

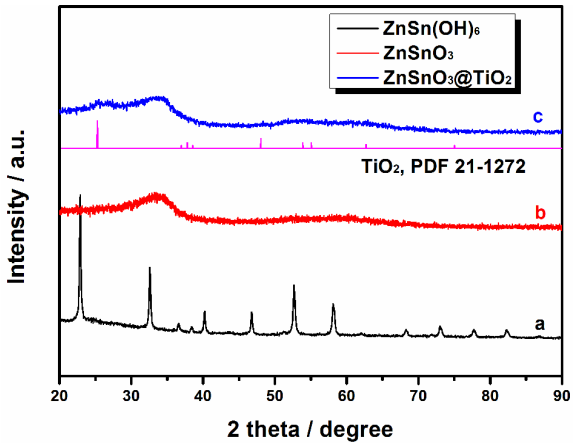

Fig. 3 XRD patterns of the prepared $ZnSn(OH)_6$, $ZnSnO_3$ and $ZnSnO_3$@TiO_2.

X-ray diffraction (XRD) patterns are used to explore the exact crystalline structure of the nanoparticles. As shown in Fig. 3, the peak of curve a is referenced to a P n3m unit cell. The 2θ values can be attributed to typical characterization diffractions of $ZnSn(OH)_6$ (Figure S3, PDF#20-1455). After the thermal treatment (450 ^{o}C), the $ZnSn(OH)_6$ nanoparticles become into $ZnSnO_3$ nanoparticles. To gain an insight into the crystalline structure evolution of the ZnSn-based nanoparticles, XRD patterns of $ZnSn(OH)_6$ nanoparticles heated at various temperature have been exhibited in Figure S3. Clearly, there is no obvious change on the diffraction peak if the $ZnSn(OH)_6$ was heated at 150 ^{o}C. However, at 200 ^{o}C, the diffraction intensity of the characteristic peak for $ZnSn(OH)_6$ decreases seriously, indicating that hydroxide has begun to decompose at this condition. The production is low-crystalline $ZnSnO_3$ at the thermal treatment of 250 - 450 ^{o}C. The crystalline $ZnSnO_3$ could not be found until at 600 ^{o}C. In Fig. 3, compared with $ZnSnO_3$ (curve b), the diffraction peak of TiO_2 could be found in $ZnSnO_3$@TiO_2 (curve c), implying that the production after thermal treatment is low-crystalline $ZnSnO_3$-TiO_2 composite materials.

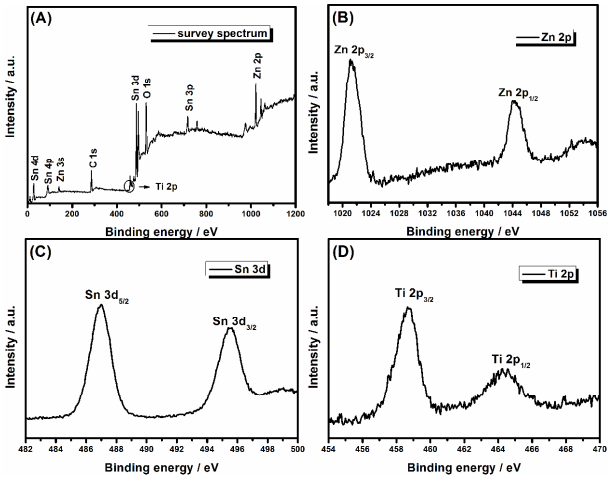

Fig. 4 (A) Survey XPS spectrum of the prepared $ZnSnO_3$@TiO_2 composite. XPS spectrum for (B) Zn 2p, (C) Sn 3d, (D) Ti 2p regions of the prepared $ZnSnO_3$@TiO_2 composite.

XPS is recognized as one useful method to token the accurate

chemical compositions and electronic structures of the nanomaterials. Fig. 4(A) shows the survey spectrum of the obtained $ZnSnO_3$@TiO_2 nanocomposite, from which could be obviously noted that the characteristic peaks of Zn, Sn, O and Ti exist in product $ZnSnO_3$@TiO_2 composite. The high-resolution XPS spectrum of Zn 2p, Sn 3d and Ti 2p orbital region for $ZnSnO_3$@TiO_2 composite are displayed in Fig. 4(B-D). As is shown in Fig. 4(B), we can find the peaks at 1021.5 eV and 1044.5 eV clearly, which is consistent with the binding energy of Zn $2p_{3/2}$ and Zn $2p_{1/2}$. The splitting energy of 23 eV between Zn $2p_{3/2}$ and Zn $2p_{1/2}$ is a typical value for Zn^{2+} in $ZnSnO_3$@TiO_2 composite. Meanwhile, the high-resolution of Sn $3d_{5/2}$ and Sn $3d_{3/2}$ XPS spectra in Fig. 4(C) can be observed obviously at 486.9 eV and 495.5 eV, respectively, which correspond to the Sn^{4+}. The characteristic peaks at 458.7 and 464.4 eV correspond to the Ti $2p_{3/2}$ and Ti $2p_{1/2}$ states (Fig. 4D), implying the presence of Ti^{4+} in TiO_2. Combining the SEM, TEM, XRD and XPS results mentioned above, a cube-like core-shell $ZnSnO_3$@TiO_2 composite structure is obtained in this method.

Electrochemical measurement

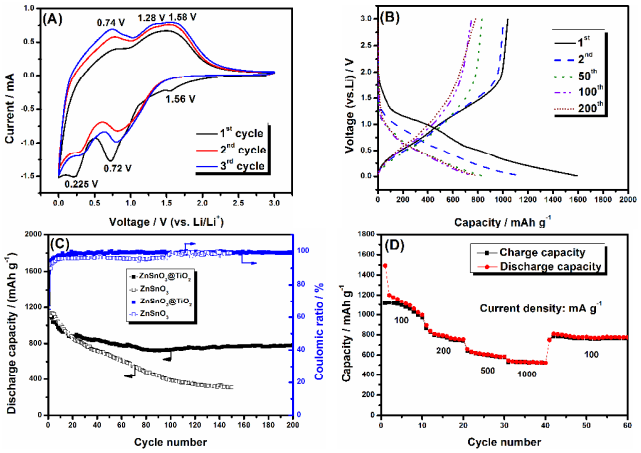

Fig. 5 (A) CVs of the electrodes at a scan speed of 0.1 mV s^{-1}. (B) Discharge-charge curves of $ZnSnO_3$@TiO_2 at a current density of 100 mA g^{-1}. (C) Coulombic efficiency and electrochemical cycling performance of the $ZnSnO_3$ and $ZnSnO_3$@TiO_2 at a current density of 100 mA g^{-1}. (D) Rate performances of the obtained $ZnSnO_3$@TiO_2

Intrigued by the structural features of $ZnSnO_3$@TiO_2 for LIB applications, various electrochemical measurements are employed as useful probe to test the lithium storage behaviours of the as-prepared $ZnSnO_3$@TiO_2. As shown in Fig. 5A, the cyclic voltammogram (CV) profiles of the prepared composite are operated at a scan rate of 0.1 mV s^{-1} over a voltage range of 0 - 3 V *versus* Li/Li^+ to understand the lithiation/delithiation mechanism. Considering that lithium storage mechanism of TiO_2 with insertion/extraction as well as $ZnSnO_3$ with the integration of alloying and conversion has been reported separately,[3a,5a,6] we proposed the following mechanism for $ZnSnO_3$@TiO_2 during discharge-charge process:

$$TiO_2 + xLi + xe\text{-} \leftrightarrow Li_xTiO_2,\ x \le 1 \quad (1)$$

$$6Li^+ + ZnSnO_3 + 6e^- \leftrightarrow Zn + Sn + 3Li_2O \quad (2)$$

$$xLi^+ + Sn + xe\text{-} \leftrightarrow Li_xSn,\ x \le 4.4 \quad (3)$$

$$yLi^+ + Zn + ye^- \leftrightarrow Li_yZn,\ y \le 1 \quad (4)$$

For $ZnSnO_3$@TiO_2 sample, in the first scan of the anode materials, an inconspicuous peak at ~1.56 V which disappeared in the subsequent cycles could be associated with a negligible amount of inserted lithium in the TiO_2 shell (Equation 1), revealing that TiO_2 in the $ZnSnO_3$@TiO_2 contributes little capacity to the hybid.[8a] A peak at 0.72 V can be attributed to the irreversible or partially reversible reduction of $ZnSnO_3$ following Equation (2) and the formation of a solid electrolyte interface (SEI) film, matching well with the upper plateau in the discharge curve. The subsequent wide peak around 0.225 V are attributed to the alloying of Zn and Sn with Li following the Equation (3) and (4). This peak shifted to ~0.33 V in subsequent scans, implying the formation of various Li_xZn and Li_ySn species.[3a] Li_xZn and Li_ySn transform into Zn and Sn at 0.74 V via a de-alloying reaction. The subsequent peaks at 1.58 V and 1.28 V derive from the partially reversible oxidation of Zn and Sn, separately.

Galvanostatic discharge/charge and cycling measurements are conducted at a current density of 100 mA g^{-1} within a cut-off window 0.01 - 3 V. The specific capacity of $ZnSnO_3$@TiO_2 is counted based on the total mass of both $ZnSnO_3$ and TiO_2. Typical voltage-specific capacity curve in Fig. 5B and Table S1 display that $ZnSnO_3$@TiO_2 delivers the first discharge capacity of 1590 mAh g^{-1} and charge capacity of 1038 mAh g^{-1}, exhibiting an initial Coulombic efficiency of 65.3%. The initial capacity loss reflects an irreversible Li^+ consumption by $ZnSnO_3$@TiO_2, which might be ascribed to the SEI formation on the mesoporous $ZnSnO_3$@TiO_2.[3,5] As a comparison, $ZnSnO_3$ shows the first discharge and charge capacities of 1680.7 and 1106 mAh g^{-1} with a Coulombic efficiency of 65.8% (Figure S4, Fig 5C). At the second cycle, the Coulombic efficiency of $ZnSnO_3$@TiO_2 increases to 94.6% dramatically. The Coulombic efficiency increases to >98% at 18th cycle, and keeps this stable efficiency at the subsequent cycles tests (up to 200th cycle). The cycle performance in Fig. 5C exhibits that $ZnSnO_3$@TiO_2 retains a reversible capacity of 780 mA g^{-1} in the 200 cycles. The results are better than the most outcomes which have been reported before.[5] In contrast, the capacity of $ZnSnO_3$ fades to 307 mA g^{-1} after 150 cycles, even it holds the higher capacity in the initial 16 cycles. On the other hand, discharge-charge curves of $ZnSnO_3$@TiO_2 at a current density of 200 mA g^{-1} also have been prepared and shown in Figure S5. It is noticeable to find that $ZnSnO_3$@TiO_2 retains a reversible capacity of 616 mAh g^{-1} after 100 cycles, which even much higher than that of $ZnSnO_3$ at the current density of 100 mA g^{-1}. Comparison of the electrochemical properties of $ZnSnO_3$ and $ZnSnO_3$@TiO_2 in Table S1 shows that $ZnSnO_3$@TiO_2 exhibits the more excellent cycle stability (>2 times on capacity) than $ZnSnO_3$.

In addition, the rate performances of $ZnSnO_3$@TiO_2 electrode are then investigated at various current densities in the range of 100 - 1000 mA g^{-1}. As shown in Fig. 5D, when cycled at 100 mA g^{-1}, $ZnSnO_3$@TiO_2 delivers a second discharge capacity of 1191.4 mAh g^{-1} and fades near 600 mAh g^{-1} after 10 cycles. During the subsequent cycles, it is distinctive to find that reversible capacities around 755, 582, 520 mAh g^{-1}, are achieved for $ZnSnO_3$@TiO_2 at current densities of 200, 500, 1000 mA g^{-1}, respectively. The results are also higher than the reported cube-like, sheet-like and Co-doped Zn_2SnO_4 materials.[5] The superiority on cycle life and rate performances might be given the credit to the stability on the structure. Figure S6 shows the EIS

spectra of $ZnSnO_3$ and $ZnSnO_3$@TiO_2 before cycle. The semicircle of $ZnSnO_3$@TiO_2 in the high-middle frequency region is little smaller than that of $ZnSnO_3$. The slope of $ZnSnO_3$@TiO_2 in the low frequency region is little higher that of $ZnSnO_3$. Therefore, the EIS results show that electrolyte and ion diffusion resistances of $ZnSnO_3$@TiO_2 are only little lower than that of $ZnSnO_3$, indicating that the enhanced cycle stability of $ZnSnO_3$@TiO_2 is mostly attributed to the enhanced structural stability.

To prove the enhanced structural stability, de-lithiated $ZnSnO_3$@TiO_2 anode after 200 cycles has been checked by SEM and TEM. As shown in Fig. 6, no obvious pulverization and agglomeration can be observed. From Figure S7, we can still find the porous structure from the nanoparticles. The granular morphology of $ZnSnO_3$@TiO_2 is well retained after the cycles test, indicating the structural completeness of nanoparticles.

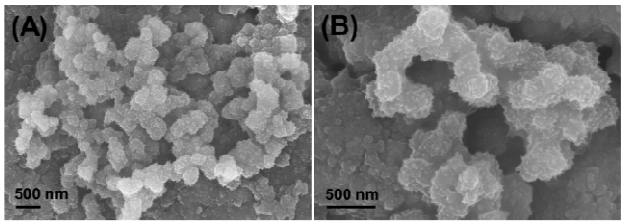

Fig. 6 SEM images of the de-lithiated $ZnSnO_3$@TiO_2 after 200 cycles.

On the basis of the above results, the enhanced cycle life of $ZnSnO_3$@TiO_2 anode can be attributed to the superiority of the hierarchical composite structure as well as the synergistic effects of $ZnSnO_3$ and TiO_2: (1) The hierarchical porous three-dimension structure can shorten the Li^+ and electrolyte molecules transportation length and heighten the electrolyte/active material contact area as well as the penetration ability of the electrolyte molecules. (2) Hierarchical porous structure can also retard the huge volume expansion during the repeated charge-discharge cycles. (3) More importantly, TiO_2 coating layer can release the stress caused by volume change originating from the conversion reaction during the insertion-extraction of Li^+ effectively. (4) The synergistic effect of the high capacity of $ZnSnO_3$ and the good structural stability of TiO_2 also contributes to the excellent electrochemical performance of the $ZnSnO_3$@TiO_2 composite.

Conclusions

In summary, a facile co-precipitation and subsequent TiO_2 coating method is used to prepare cube-like interconnected amorphous $ZnSnO_3$@TiO_2 nanocomposites. The integration of an interconnected TiO_2 wrapping and abundant mesopores releases the stress of volume expansion, resulting in a significantly enhanced electrochemical stability performance. Furthermore, the amorphous nature of the $ZnSnO_3$@TiO_2 with loose micro-framework could facilitate Li-ion diffusion among the active material. As a result, the as-prepared $ZnSnO_3$@TiO_2 nanocomposites exhibit excellent cycle stability and rate capability for lithium storage in comparison with $ZnSnO_3$. This described synthetic strategy could motivate further exploration of multiple components and structures for next-generation high-performance LIBs or other fields of energy storage and conversion.

Acknowledgements

This research is financially supported by the National Nature Science Foundation of China (Grant No. 20111061).

Notes and references

[a] *State Key Laboratory of Rare Earth Resource Utilization, Changchun Institute of Applied Chemistry, Changchun 130022, Jilin, China. E-mail: lmwang@ciac.ac.cn*
[b] *Changzhou Institute of Energy Storage Materials & Devices,Changzhou 213000, Jiangsu, China*
[c] *University of Chinese Academy of Sciences, Beijing 100049, China*
E-mail: ylqin@ciac.ac.cn

† Electronic Supplementary Information (ESI) available: [more details of SEM images, XRD spectrum and LIBs performance]. See DOI: 10.1039/b000000x/

1 (a) P. G. Bruce, B. Scrosati and J. M. Tarascon, *Angew. Chem.,* 2008, **120**, 2972; (b) L. W. Ji, Z. Lin, M. Alcoutlabi and X. W. Zhang, *Energy Environ. Sci.,* 2011, **4**, 2682; (c) Y. Lu, J. P. Tu, Q. Q. Xiong, J. Y. Xiang, Y. J. Mai, J. Zhang, Y. Q. Qiao, X. L. Wang, C. D. Gu and S. X. Mao, *Adv. Funct. Mater.,* 2012, **22**, 3927; (d) Q. Q. Xiong, J. P. Tu, X. H. Xia, X. Y. Zhao, C. D. Gu and X. L. Wang, *Nanoscale,* 2013, **5**, 7906.

2 (a) Y. Inaguma, M. Yoshida and T. Katsumata, *J. Am. Chem. Soc*., 2008, **130**, 6704; (b) C. H. Fang, B. Y. Geng, J. Liu and F. M. Zhan, *Chem. Commun.*, 2009, 2350; (c) T. Lana-Villarreal, G. Boschloo and A. Hagfeldt, *J. Phys. Chem. C*, 2007, **111**, 5549; (d) B. Y. Geng, C. H. Fang, F. M. Zhan and N. Yu, *Small*, 2008, **4**, 1337; (e) D. L. Young, H. Moutinho, Y. Yan and T. J. Coutts, *J. Appl. Phys.*,2002, **92**, 310; (f) L. Han, J. Liu, Z. Wang, K. Zhang, H. Luo, B. Xu, X. Zou, X. Zheng, B. Ye and X. Yu, *CrystEngComm*, 2012, **14**, 3380.

3 (a) F. Han, W. C. Li, C. Lei, B. He, K. Oshida and A. H. Lu, *Small*, 2014, **10**, 2637; (b) J. M. Wu, C. Xu, Y. Zhang and Z. L. Wang, *ACS Nano,* 2012, **6**, 4335; (c) J. M. Wu, C. Xu, Y. Zhang, Y. Yang, Y. Zhou and Z. L. Wang, *Adv. Mater*., 2012, **24**, 6094.

4 (a) S. H. Choi and Y. C. Kang, *ChemSusChem*, 2013. **63**, 2111; (b) Z. Wang, Z. Wang, W. Liu, W. Xiao and X. W. Lou, *Energy Environ. Sci*., 2013, **6**, 87; (c) M. V. Reddy, G. V. S. Rao and B. V. R. Chowdari, *Chem. Rev.,* 2013, **113**. 5364.

5 (a) Y. Chen, B. Qu, L. Mei, D. Lei, L. Chen, Q. Li and T. Wang, *J. Mater. Chem.*, 2012, **22**, 25373; (b) J. F. Duan, S. C. Hou, S. G. Chen and H. G. Duan, *Mater. Lett.*, 2014, **122**, 261; (c) H. Wang, B. Y. Wang, J. Meng, J. Wang and Q. C. Jiang, *J. Mater. Chem. A*, 2014, DOI**:** 10.1039/C4TA03144J.

6 (a) J. Jin, S. Z. Huang, J. Liu, Y. Li, D. S. Chen, H. E. Wang, Y. Yu, L. H. Chen and B. L. Su, *J. Mater. Chem. A*, 2014, **2**, 9699; (b) J. S. Chen, L. A. Archer and X. W. Lou, *J. Mater. Chem.,* 2011, **21**, 9912; (c) F. F. Cao, Y. G. Guo and L. J. Wan, *Energy Environ. Sci*., 2011, **4**, 1634; (d) H. Cao, B. Li, J. Zhang, F. Lian, X. Kong and M. Qu, *J. Mater. Chem.,* 2012, **22**, 9759.

7 (a) Y. Luo, J. Luo, W. Zhou, X. Qi, H. Zhang, D. Y. W. Yu, C. M. Li, H. J. Fan and T. Yu, *J. Mater. Chem. A,* 2013, **1**, 273; (b) C. Zha, D. He, J. Zou, L. Shen, X. Zhang, Y. Wang, H. H. Kung and N. Bao, *J. Mater. Chem. A,* 2014, **2**, 16931; (c) Z. Hong and M. Wei, *J. Mater. Chem. A,* 2013, **1**, 4403; (d) Y.Yan, B. Hao, D. Wang, G. Chen, E. Markweg, A. Albrecht and P. Schaaf, *J. Mater. Chem. A,* 2013, **1**, 14507.

8 (a) Y. Tang, D. Wu, S. Chen, F. Zhang, J. Jia and X. Feng, *Energy Environ. Sci*., 2013, **6**, 2447; (b) Q. Tian, Z. Zhang, L. Yang and S. I. Hirano, *J. Power Sources*, 2014, **253**, 9; (c) Z. Wang, Z. C. Wang, S. Madhavi and X. W. Lou, *Chem. Eur. J.* 2012, **18**, 7561; (d) X. Zhang, H. Chen, Y. Xie and J. Guo, *J. Mater. Chem. A,* 2014, 2, 3912; (e) J. Liu, D. Qian, H. Feng, J. Li, J. Jiang, S. Peng and Y. Liu, *J. Mater. Chem. A,* 2014, **2**, 11372.

Table of contents

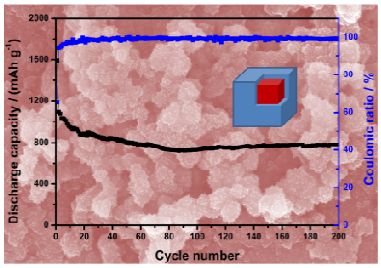

Cube-like porous $ZnSnO_3$@TiO_2 has been prepared. Furthermore, it exhibits the excellent cycle stability and rate capability for LIBs.